J. Phys. D: Appl. Phys. **42** (2009) 015304 (7pp) doi:10.1088/0022-3727/42/1/015304

On the relationship between the peak target current and the morphology of chromium nitride thin films deposited by reactive high power pulsed magnetron sputtering

J Alami[1], K Sarakinos[2], F Uslu and M Wuttig

Institute of Physics (IA), RWTH Aachen University, D 52056 Aachen, Germany

E-mail: sarakinos@mch.rwth-aachen.de (K Sarakinos)

Received 8 August 2008, in final form 21 October 2008
Published 10 December 2008
Online at stacks.iop.org/JPhysD/42/015304

Abstract

High power pulsed magnetron sputtering (HPPMS) is used to deposit CrN films without external heating at different peak target currents, while the average current is kept constant. Films are also grown by dc magnetron sputtering (dcMS), for reference. The plasma properties, the deposition rate and the morphology of the films are investigated. The plasma analysis reveals that HPPMS provides higher fluxes of ionized species (both gas and sputtered) to the growing film, as compared with dcMS. In addition, the ionic bombardment during HPPMS increases, when the peak target current is increased. The HPPMS films exhibit changes of the density and the surface roughness as the peak target current increased, while the deposition rate decreases drastically. Furthermore, it is found that different thin-film morphologies are obtained starting from a porous columnar morphology for the dcMS films, which turns to a dense columnar one at low peak target currents and ends up to a featureless morphology at high peak target currents for the films grown by HPPMS. A new structure zone model specific for high ionization sputtering is, therefore, outlined.

1. Introduction

Physical vapour deposition is a well-established thin-film technology, in which the variation of the deposition parameters enables the control of the thermodynamic and the kinetic conditions during the film growth [1]. This affects the morphology of the films [1, 2] and provides means for altering their optical, electrical and mechanical properties [3–5]. One way to understand the effect of the deposition parameters variations on the growth of thin films is by classifying the different morphologies in a so-called structure zone model (SZM) [6]. For example, in films grown by evaporation this classification can be based upon the substrate temperature. However, when growth is performed by magnetron sputtering techniques, modifications of this classical ZSM are necessary [7, 8]. This is due to the presence of low-flux ionic energetic bombardment during magnetron sputtering [2, 9–11]. Other deposition techniques, where higher fluxes of ions are available, has been shown by a number of authors [12–15] to further modify the morphological features predicted by the classical SZMs.

It is, therefore, evident that the presence of ions in the deposition flux is beneficial, since it allows for control and tailoring of the film properties over a wide range. High power pulsed magnetron sputtering (HPPMS) [16–21] is a newly developed high ionization deposition technique. Typical for HPPMS are the high peak power unipolar pulses of a few tens of microseconds, which are supplied to the target (cathode),

[1] Present address: Sulzer Metaplas GmbH, Am Böttcherbrg 30-38, 51427 Bergisch Gladbach, Germany.
[2] Present address: Materials Chemistry, RWTH Aachen University, Mies-van-der-Rohe-Straße 10, 52074 Aachen, Germany.

 © 2009 IOP Publishing Ltd Printed in the UK

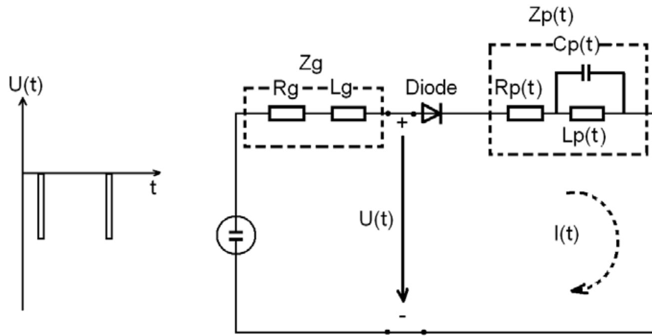

Figure 1. The electrical circuit representing the HPPMS deposition system.

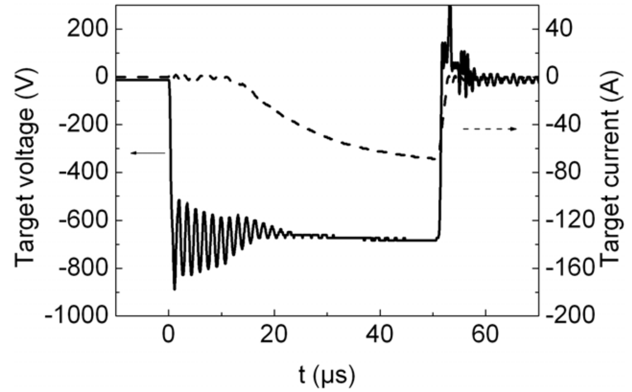

Figure 2. Temporal evolution of the target voltage and current density during HPPMS. It is seen that the current is measured some microseconds after the pulse initiation as a result of the plasma build-up.

resulting in high plasma (electron) densities [22] and a high ionization of the sputtered material [16, 23, 24]. In general, the ionization fraction in HPPMS is much higher than the value of ∼1% typically obtained by dcMS, and depends on the target material, the sputtering gas, the pressure and the peak target power [22]. The increased ionization obtained by HPPMS has been utilized to enhance the film properties, including density, surface roughness [25], optical performance [26, 27] and electrical conductivity [28]. HPPMS has also been shown to provide means for tailoring the microstructure [29–31] and composition [32] of the growing film. In most of these investigations HPPMS has been used by choosing arbitrary values for the pulse on-time and off-time. In a recent study, we have shown [33] that the chosen pulse on/off time configuration considerably affects the plasma conditions and the deposition rate. However, the effect of the pulse on/off time configuration on the morphology of the grown films has not been studied. This is investigated in this work by growing CrN films by HPPMS and analysing their properties.

CrN is known for its refractory character and its exceptional mechanical properties [34, 35]. CrN thin films are routinely used as hard coatings, and for applications in severe environments, due to their, relatively, high hardness and chemical stability. In addition, CrN behaves as a semiconductor [36, 37] with the single crystal (1 0 0) CrN having an optical gap of ∼0.7 eV [36]. In this study, CrN films are deposited by unipolar HPPMS using a number of pulse on/off time configurations. Films are also grown by dc magnetron sputtering (dcMS), for reference. The resulting changes in the morphology of the films are identified and discussed in the light of the energetic bombardment provided at the various deposition conditions.

2. Experimental procedure

2.1. Deposition setup

The power device used in this work consisted of a conventional Advanced Energy Pinnacle dc power supply connected to a MELEK SPIK 2000A pulsing unit [38]. An electric/electronic equivalent network diagram of the magnetron deposition system can be a diode with a complex impedance $Z_p(t)$, as shown in figure 1. The pulse current is then a function of the time-dependent impedance $Z_p(t)$. Due to the very low generator impedance, Z_g, the applied power can be directly transferred to the target without significant losses. This mode of operation results in a constant voltage during the pulse on-time. The target voltage obtains, thus, a rectangular-like shape, while the discharge current shows a saw tooth like shape [38]. The time-dependent target current and voltage were measured using a LEM LA205-S current transducer and a LEM CV3-1500 voltage transducer, respectively, and were monitored in a TDS2014 digital oscilloscope. An example of the time-dependent current and voltage curves is shown in figure 2, where it is also seen that no current is measured in the first 20 μs from the pulse start, accompanied by voltage oscillations of a few hundred volts. This is due to the high impedance prior to the ignition of the plasma which results from the complete 'dying out' of the discharge between pulses [39]. This has been shown by Gudmundsson *et al* [39] to be a function of the chamber pressure. In fact, when the discharge pressure was increased, a faster ignition and a decrease in the ripple time were observed [39].

2.2. Plasma analysis

The effect of the deposition parameters on the discharge properties was studied by performing plasma measurements using a Langmuir probe [40] placed at the substrate's position. Time-resolved curves of the probe current (I_{pr}) were recorded for each applied probe voltage (V_{pr}) with steps of 0.5 V. The data were processed using MATLAB software tools [41] and the electron density n_e, electron temperature T_e, as well as the plasma potential V_p and the floating potential V_f were determined, according to Liebermann and Lichtenberg [42]. The ion flux to the substrate was also estimated by measuring the ion saturation current using a flat probe at the substrate position. Details on the construction of the Langmuir and the flat probes are given elsewhere [39]. In order to investigate the changes in the plasma composition with changing deposition conditions, time-resolved optical emission spectroscopy (OES) measurements were performed. A Mechelle 5000 Spectrometer equipped with an intensified CCD camera for optimized signal count was used for the purpose. Light emission signals were collected using a

fiber optic placed 30 cm from the target surface, at a 45° angle. The OES measurements were carried out by measuring the emission intensity corresponding to the four wavelengths 283.56 nm, 301.73 nm, 487.89 nm and 696.53 nm, representing Cr^+, Cr^0Ar^+ and Ar^0 species [43], respectively.

2.3. Film deposition and characterization

CrN films were deposited without external heating on Si (1 0 0) substrates placed at a distance of 70 mm from a Cr target that had a diameter of 75 mm and a thickness of 6.3 mm. The temperature measurements, performed during the growth indicated that the substrate temperature during HPPMS was independent of the choice of the pulse on/off time configuration, and was only slightly higher than that during dcMS (130 °C as opposed to 110 °C for dcMS). The Si substrates were cleaned sequentially in tetrachloroethylene, acetone and isopropanol ultrasonic baths and then blown dry with a nitrogen gas, prior to introducing them inside the chamber. Ar (99.999%) gas and N_2 (99.999%) mixtures with a total pressure of 0.8 Pa were used as a working gas. Measurements of the target voltage evolution as a function of the N_2 flow were performed (not shown here), in order to determine the working point for depositions. Trial depositions showed that in order to obtain stoichiometric CrN films, a N_2 flow of 30 sccm was needed for dcMS. At a N_2 flow of 25 sccm or lower, the films contained the Cr_2N phase beside the CrN phase. For the HPPMS depositions, N_2 flows lower (than those used for dcMS) were needed in order to obtain single phased CrN films. All depositions were, however, performed at a N_2 flow of 30 sccm, in order to ensure that the grown films will not contain Cr_2N. For the HPPMS depositions, high power unipolar pulses of a few hundred W cm^{-2} were applied to the target with a pulse on-time of 50 μs and duty times ranging between 2% and 25%. The decrease in the duty cycle from 25% down to 2% resulted in an increase in the peak target current (I_{Tp}) from 6 to 180 A to keep the average current constant at 0.9 A. These values corresponded to peak target current densities in the range between 0.15 and 4.2 A cm^{-2}. Films of 250 to 500 nm in thickness were deposited on grounded substrates by HPPMS and by dcMS, for reference. It has to be mentioned here that the decrease in the duty cycle resulted in an increase in the target voltage. Thus, the average power was increased, since the depositions were performed at a constant average target current.

In order to examine the films' properties x-ray measurements were performed using a Philips X'Pert diffractometer. The films' thickness, root mean square roughness (σ) and density (ρ) were determined by means of x-ray reflectometry (XRR) by fitting the measured XRR curves to simulated ones using the WINGIXA software package [44]. The crystal structure and the phase composition of the films were evaluated using x-ray diffractometry (XRD) in both Bragg–Brentano (BB) and grazing incidence (GI) geometries. Electron microscopy in transmission (TEM) and scanning (SEM) modes was used in order to investigate the films' microstructure and morphology. Cross-sectional samples for SEM were prepared by cutting the samples so as to obtain a brittle fracture in the CrN films. SEM was carried out using a Jeol JSM-7400F equipped with a field emission gun. Cross-sectional TEM samples were prepared using standard mechanical thinning procedures followed by low angle Ar ion milling at incident angles of 8° to 10° using a BalTec RES101 system. The specimens were thinned from both sides with a high tension of 5 kV and a gun current of 1 mA. TEM analysis was carried out using a Philips CM 20 transmission electron microscope, operated at 200 kV with a 0.24 nm point resolution. The microstructure was investigated by means of Fresnel fringe analysis, in order to reveal possible porous film regions. In all imaging modes the orientation of the electron beam was parallel to the ⟨1 1 1⟩ direction of the Si substrate.

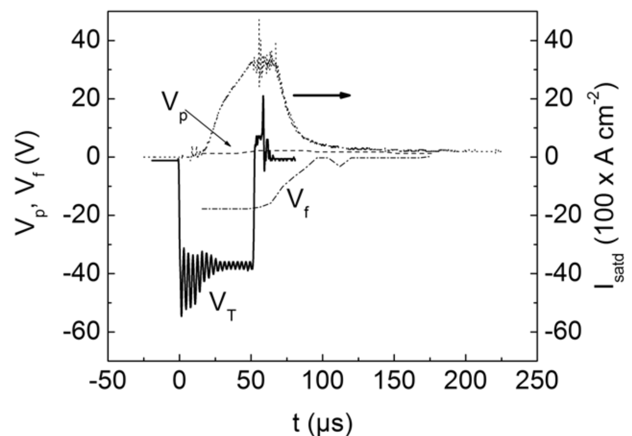

Figure 3. Plasma and floating potentials as well as ion saturation current measured during and after the pulse on-time. The target voltage is also shown in thick lines.

3. Results

3.1. Plasma analysis

The electron density n_e was measured in the substrate's vicinity for the HPPMS discharge with the pulse on/off time configuration 50/2450 (corresponding to a duty cycle of 2%) and was found to reach a peak value of 7×10^{17} cm^{-3}. This value was more than 2 orders of magnitude higher than the value of 4×10^{15} cm^{-3} measured for the dcMS discharge operating at the same average target current. The plasma and the floating potentials measurements, presented in figure 3, showed that the V_f had a value of ~ -18 V during the pulse on-time, but decreased fast after the pulse was switched off to reach a value near zero. The plasma potential, on the other hand, was nearly constant with a value between 1 and 2 V. The plasma and floating potentials could not be reliably measured in the first 10 μs of the pulse as the plasma was unstable during the early build-up stage. The time-dependent mean electron energy was calculated and was shown to decrease from ~4 eV at 20 μs after the pulse initiation to ~2 eV at the end of the pulse on-time, and to 0.5 eV a few tens of microseconds after the pulse was switched off. This behaviour indicates a thermalization of the plasma species as they arrive at the substrate's vicinity. The peak ion flux estimated from

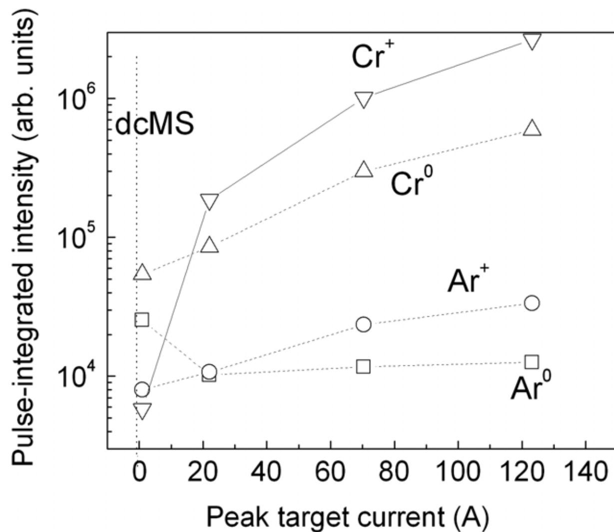

Figure 4. Pulse-integrated intensity of Ar^0 (squares), Ar^+ (circles), Cr^0 (triangles) and Cr^+ (inverse triangles) emission lines as a function of the peak target current. The emission intensity during dcMS is also plotted for $I_{Tp} = 0$ A.

the ion saturation current density measurements (shown in figure 3) was 2–3 orders of magnitude higher than during dcMS. However, because of the large distance between the target and the substrate (70 mm), a significant number of ions reached the substrate tens of microseconds after the pulse was switched off. Consequently, the accelerating voltage that the ions were subjected to at the substrate–plasma sheath ranged between $\Delta V = V_p - V_f \sim 1$ V for the majority slow thermalized ions and $\Delta V \sim 20$ V for the minority fast hot ions. An increase in the target peak current (induced by an increase in the pulse off-time) resulted in an increase in the ion flux to the target, while the plasma potentials only marginally changed.

The OES measurements performed for both the HPPMS and the dcMS discharges revealed that the HPPMS discharge exhibited a significantly higher emission intensity of the ionized Cr^+ and Ar^+ species. The time-resolved emission intensities for ionized and neutral Cr and Ar species were integrated over the pulse time and are presented in figure 4 as functions of the peak target current (I_{Tp}). It is seen that at $I_{Tp} \sim 120$ A, the HPPMS emission signal intensity of Cr^+ (10^6 counts) was 2 orders of magnitude higher than the dcMS value ($I_{Tp} = 0$) of less than 10^4 counts. Furthermore, the intensity of the Ar^+ species increased from a value of $\sim 10^4$ counts at dcMS up to a value of 5×10^4 counts at $I_{Tp} = 120$ A, i.e. the increase in the peak target current resulted in higher Cr^+/Ar^+ intensity ratios. Finally, the Ar^0 species exhibited a slight intensity decrease. This behaviour is, as discussed in an earlier work [33], a result of the gas rarefaction.

3.2. Film roughness, density and deposition rate

The XRR measurements demonstrated that the film roughness σ decreased from the dcMS value of 2.7 nm to a HPPMS value of $\sigma \sim 0.5$ nm which was obtained at a peak current value of $I_{Tp} \sim 44$ A. Increasing the peak current further did not affect the film roughness. The film density ρ exhibited an increase from 5.70 g cm^{-3} (dcMS) to 6.05 g cm^{-3} for the HPPMS film grown at $I_{Tp} \sim 44$ A. Here too, no change in ρ was observed at higher I_{Tp} values. The deposition rates, R_d, calculated from the XRR measurements showed that R_d was 0.5 nm s^{-1} at $I_{Tp} \sim 44$ A, which was close to the value obtained by dcMS. As I_{Tp} increased, R_d dropped further until it reached a value of 0.28 nm s^{-1} for $I_{Tp} \sim 180$ A.

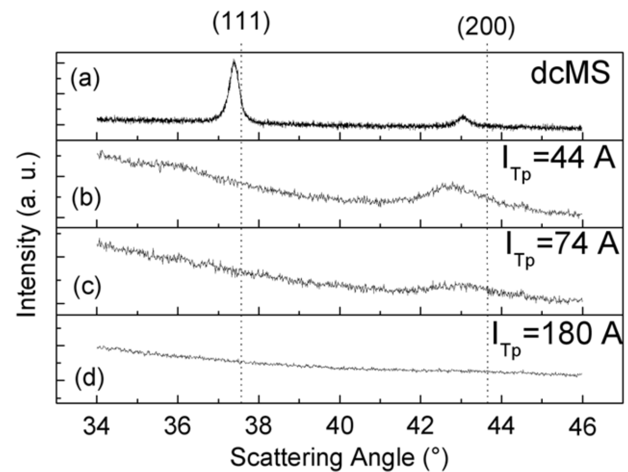

Figure 5. X-ray diffraction patterns of (*a*) dcMS and HPPMS films grown at the peak target current values of (*b*) 44 A (*c*) 74 A and (*d*) 180 A. The position of the (1 1 1) and (2 0 0) reflections in the unstrained bulk CrN is designated with vertical dotted lines.

3.3. Film morphology

The BB-XRD patterns corresponding to samples grown at the various deposition conditions are presented in figure 5. The measurements revealed that the dcMS grown film exhibited the CrN crystal structure with a strong (1 1 1) and a weak (2 0 0) reflection. The BB patterns of the samples deposited by HPPMS exhibited much broader reflections, in comparison with the dcMS sample, with an intensity that became weaker and finally disappeared when the peak target current was increased.

The cross-sectional SEM micrographs shown in figure 6 display the morphologies for the dcMS film and for HPPMS films grown at the three different I_{Tp} values. It is seen that the dcMS film (figure 6(*a*)) exhibited a columnar competitive growth. The corresponding higher magnified TEM micrograph shown in figure 7(*a*) revealed further that the structure was quite porous and could be described as belonging to zone 1 in the SZM growth model [6, 7]. When HPPMS was used, a distinct change in the morphology was seen. At a low I_{Tp} value of 44 A (figure 6(*b*)), the film still exhibited a dense columnar structure but thinner columns. Furthermore, the corresponding TEM micrograph shown in figure 7(*b*) displayed no porosity in the film. As I_{Tp} was increased to 74 A (figure 6(*c*)), a featureless morphology was obtained, while the high density was still maintained. Similar morphology was also observed in figure 6(*d*) which corresponds to $I_{Tp} =$ 180 A. The corresponding TEM micrograph (figure 7(*c*)) also exhibited a non-porous featureless structure, indicating a dense

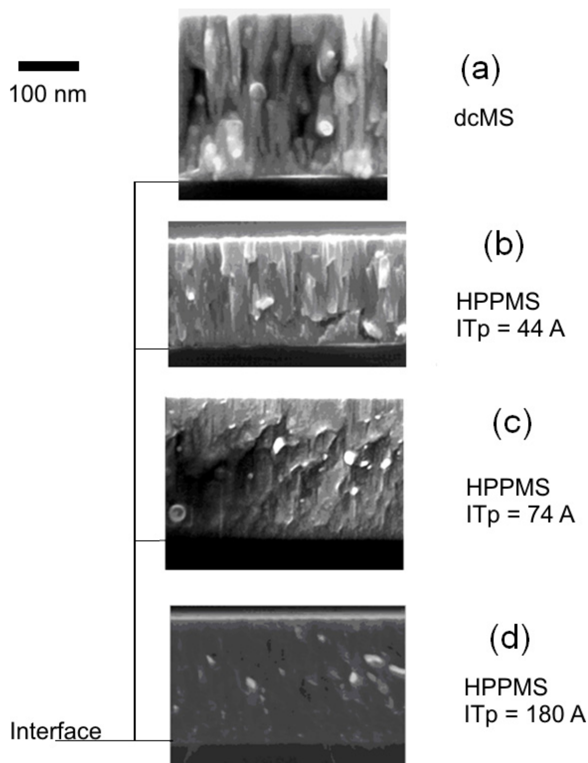

Figure 6. SEM micrographs of (*a*) dcMS and HPPMS films grown at the peak target current values of (*b*) 44 A (*c*) 74 A and (*d*) 180 A. The dcMS film shows a columnar competitive growth typical for zone 1 and zone T. The HPPMS films exhibit a dense columnar structure which turns into a nanocrystalline one when the peak target current is increased.

morphology. The selected area electron diffraction patterns, shown in the inset of the TEM micrographs in figure 7, revealed that the diffraction rings were more diffuse for higher values of peak target current. The latter, in combination to the results presented in figures 5 and 6, was indicative of a transition from polycrystalline to nanocrystalline films, when the peak target current was increased.

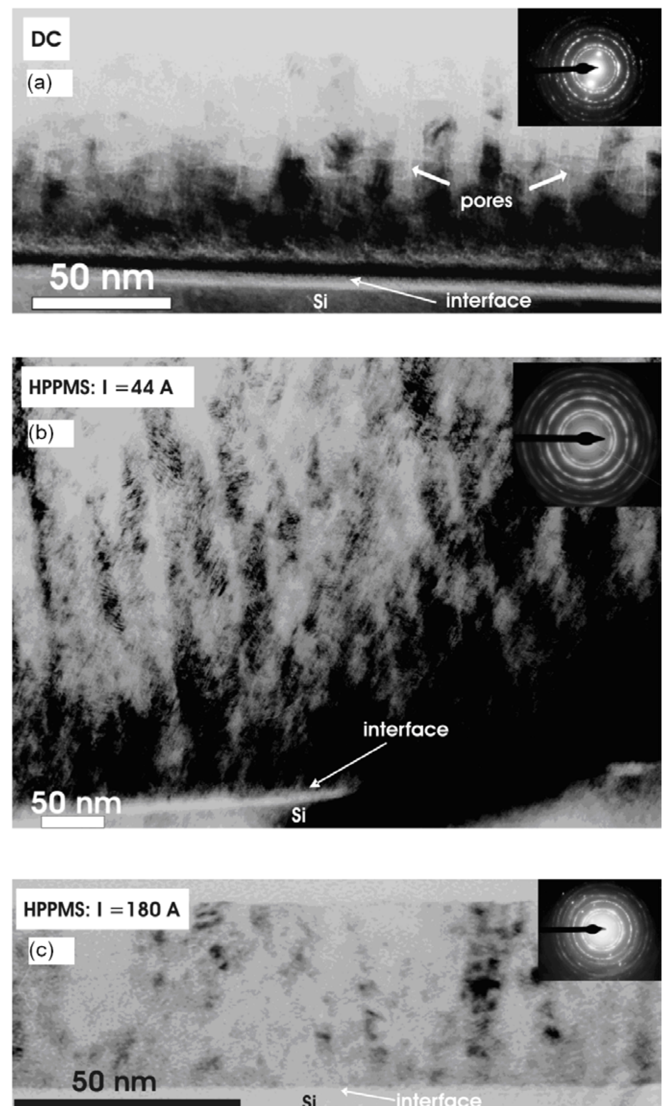

Figure 7. TEM micrographs of (*a*) dcMS and HPPMS films grown at the peak target current values of (*b*) 44 A and (*c*) 180 A.

4. Discussion

As mentioned in section 2.3, all films were deposited without external heating of the substrate. The temperature induced on the substrate as a result of the interaction of the growing film with the plasma (110 °C–130 °C) corresponds to a homologous temperature T_s/T_m (T_s is the substrate in Kelvin and T_m is the melting temperature of the deposited material also in Kelvin) of ∼0.28 [45]. These conditions give rise to film morphologies which can be classified in zones 1 and/or T of the SZM [2, 46], i.e. consist of V-shaped columns (as a result of competitive growth) and significant inter-columnar porosity [2, 46]. These features were indeed observed for the dcMS grown films (figures 6(*a*) and 7(*a*)). On the other hand, the morphology of the HPPMS films showed transition from a dense columnar morphology to a nanocrystalline featureless one as the peak target current, was increased. The relatively high values of ion saturation current measured for HPPMS (2–3 orders of magnitude higher than those in dcMS) imply that this technique can provide high fluxes of ionized species to the growing film. In addition, the flux of these species increases when the peak target current is increased, as mentioned in section 3.1. The ions in HPPMS exhibit, in general, a broad energy distribution [23] during the pulse on-time. However, in their majority they are nearly thermalized as they make their way from the target to the substrate [22]. This is confirmed by the low electron temperature measured during and, especially, after the pulse-end. Moreover, the increase in the Cr^+/Ar^+ emission intensity ratio (section 3.1) speaks of an enhancement of the fraction of the metal ions in front of the target, when the peak target current is increased. It is thus seen that a variety of low-energy ion-irradiation conditions, with respect to the flux and the nature of the bombarding ionized species, could be provided depending on the pulse on/off time configuration (i.e. peak target current). The increase in the total bombarding flux and of the fraction of Cr^+ species (induced by an increase in the peak target current) led to a drop in the surface roughness and a densification of the films, as demonstrated in section 3.2. This

behaviour is an indication of an enhanced surface diffusion length of the adatoms [47, 48]. The latter can be explained by the increase in the average energy provided per deposited atoms, caused by the higher flux of bombarding species [48]. In addition, the increase in the Cr^{+} fraction in the total flux results in a more efficient momentum transfer to the adatoms, contributing further to the enhanced adatom mobility [48]. The increase in the flux of the low-energy bombarding species can also explain the morphological features observed in section 3.3. Petrov *et al* [2] and Barna *et al* [46] have explained that ion irradiation leads to periodical interruption of the individual grain growth and induces surface defects promoting in such a way, secondary nucleation (re-nucleation). These mechanisms are consistent with the transition from a dense columnar structure to a nanocrystalline one, when the peak target current is increased (figures 5–7). It has to be mentioned here that in conventional sputtering techniques secondary nucleation, which leads to dense equiaxed morphologies, can only be promoted by high growth temperatures and is a result of bulk diffusion [6, 7]. It is therefore evident that the low-energy high-flux ion irradiation during HPPMS can be used, in order to overcome the characteristically rough and under-dense microstructures of zones I and T in the SZM model deposited at low substrate temperatures (typically $T_s/T_m < 0.3$) [6, 7] and obtain morphologies unique for low temperature deposition. This work thus presents an outline for a new SZM specific for high ionization sputtering at ambient temperatures.

The results presented in this work show that all the HPPMS films had better properties than the dcMS film. However, although the morphology showed clear changes with peak target current, the film density and surface roughness did not change much. On the other hand, the deposition rate decreased dramatically with increasing peak target current. This is known also from other works and is a characteristic of HPPMS as a result of the increased self-sputtering with increasing ionization [33]. It is therefore important to see the obtained film properties in the context of deposition rate gains.

5. Conclusions

In this study, HPPMS was used to deposit CrN films at different peak target current, while keeping the average current constant. The HPPMS films' properties were compared with dcMS grown films. In order to understand the effect of ion bombardment on the morphology and film properties, the CrN thin films were grown without external heating. As a result, a new SZM specific for high ionization sputtering was outlined, where it was shown that for the same average current, the morphology of the films changes from columnar to featureless as the target peak current increases. Furthermore, the HPPMS films showed little change in the density and the surface smoothness as the peak target current increased, suggesting that the high density and low surface roughness of the CrN, could be obtained at a high deposition rate close to that of dcMS.

Acknowledgments

This work has been supported by the Deutsche Forschungsgemeinschaft (WU 243/9). Mr Günter Mark (MELEC GmbH) is acknowledged for technical assistance with the pulsing unit.

References

[1] Ohring M 1992 *The Material Science of Thin Films* (New York: Academic)
[2] Petrov I, Barna P B, Hultman L and Greene J E 2003 *J. Vac. Sci. Technol.* A **21** 117
[3] Rickerby D S and Bell S J 1989 *Surf. Coat. Technol.* **39/40** 315
[4] Krusin-Elbaum L, Ahn K, Souk J H, Ting C Y and Nesbit L A 1986 *J. Vac. Sci. Technol.* A **4** 3106
[5] Lobl P, Huppertz M and Mergel D 1994 *Thin Solid Films* **251** 72
[6] Movchan B A and Demchishin A V 1969 *Fiz. Met. Mettaloved.* **28** 83
[7] Thornton J A 1974 *J. Vac. Sci. Technol.* **11** 666
[8] Messier R, Giri A P and Roy R A 1984 *J. Vac. Sci. Technol.* A **2** 500
[9] Savvides N and Bell T J 1992 *J. Appl. Phys.* **72** 2791
[10] Petrov I, Abibi F, Greene J E, Sproul W D and Munz W-D 1992 *J. Vac. Sci. Technol.* A **10** 3283
[11] Hultman L, Munz W-D, Musil J, Kadlec S, Petrov I and Greene J E 1991 *J. Vac. Sci. Technol.* A **9** 434
[12] Schneider J M, Rohde S, Sproul W D and Matthews A 2000 *J. Phys. D: Appl. Phys.* **33** R173
[13] Ehiasarian A P, Anders A and Petrov I 2007 *J. Vac. Sci. Technol.* A **25** 543
[14] Schneider J M, Sproul W D, Chia R W J, Ming-Show Wong and Matthews A 1997 *Surf. Coat. Technol.* **96** 262
[15] Schneider J M, Sproul W D, Voevodin A A and Matthews A 1997 *J. Vac. Sci. Technol.* A **15** 1084
[16] Kouznetsov V, Macák K, Schneider J M, Helmersson U and Petrov I 1999 *Surf. Coat. Technol.* **122** 290
[17] Gudmundsson J T, Alami J and Helmersson U 2001 *Appl. Phys. Lett.* **78** 3427
[18] Gulfason K B, Alami J, Gudmundsson J T and Helmersson U 2005 *J. Phys. D: Appl. Phys.* **38** 3417
[19] Ehiasarian A P, New R, Münz W-D, Hultman L, Helmersson U and Kouznetsov V 2002 *Vacuum* **65** 147
[20] Sproul W D, Christie D J and Carter D C 2004 *Society of Vacuum Coaters 47th Annual Technical Conf. Proc. (Dallas, TX)* p 96
[21] Konstantinidis S, Dauchot J P, Ganciu M and Hecq M 2006 *Appl. Phys. Lett.* **88** 021502
[22] Alami J, Gudmundsson J T, Böhlmark J and Helmersson U 2005 *Plasma Sources. Sci. Technol.* **14** 525
[23] Bohlmark J, Alami J, Ehiasarian A P, Christou C and Helmersson U 2005 *J. Vac. Sci. Technol.* A **23** 18
[24] Dekoven B M, Ward P R, Weiss R E, Christie D J, Scholl R A, Sproul W D, Tomasel F and Anders A 2003 *Society of Vacuum Coaters, 46th Annual Technical Conf. Proc.* p 158
[25] Alami J, Persson P O Å, Böhlmark J, Gudmundsson J T, Music D and Helmersson U 2005 *J. Vac. Sci. Technol.* A **23** 278
[26] Sarakinos K, Alami J and Wuttig M 2007 *J. Phys. D: Appl. Phys.* **40** 2108
[27] Davis J A, Sproul W D, Christie D J and Geisler M 2005 *Society of Vacuum Coaters 47th Annual Technical Conf. Proc. (Dallas, TX)* p 215
[28] Sarakinos K, Woerdenweber J, Uslu F, Sulz P, Alami J and Wuttig M 2008 *Surf. Coat. Technol.* **202** 2323

[29] Ehiasarian A P, Munz W-D, Hultman L, Helmersson U and Petrov I 2003 *Surf. Coat. Technol.* **163–164** 267
[30] Alami J, Eklund P, Andersson J M, Lattemann M, Wallin E, Bohlmark J, Persson P and Helmersson U 2007 *Thin Solid Films* **515** 3434
[31] Konstantinidis S, Dauchot J and Hecq M 2006 *Thin Solid Films* **515**
[32] Alami J, Eklund P, Emmerlich J, Jansson U, Wilhelmsson O, Högberg H, Hultman L and Helmersson U 2006 *Thin Solid Films* **515** 1731
[33] Alami J, Sarakinos K, Mark G and Wuttig M 2006 *Appl. Phys. Lett.* **89** 154104
[34] Glocker D A and Shat S I 1995 *Handbook of Thin Film Process Technology* (Wilmington, DE: Institute of Physics)
[35] Navansek B, Panjan P and Milosev I 1997 *Surf. Coat. Technol.* **97** 182
[36] Gall D, Shin C-S, Haasch R T, Petrov I and Greene J E 2002 *J. Appl. Phys.* **91** 5882
[37] Logothetidis S, Patsalas P, Sarakinos K, Charitidis C and Metaxa C 2004 *Surf. Coat. Technol.* **180–181** 637
[38] MELEC GmbH *US Patent No* US 6,735,099 B2
[39] Gudmundsson J T, Alami J and Helmersson U 2002 *Surf. Coat. Technol.* **161** 249
[40] Langmuir I 1929 *Phys. Rev.* **33** 954
[41] Gudmundsson J T 1997 *Smoothing of the I–V Langmuir Characteristic Memorendum No UCB/ERL M97/38* Electron Research Laberatory, University of California Berkeley
[42] Lieberman M A and Lichtenberg A J 1994 *Principles of Plasma Discharges and Materials Processing* (Wiley: New York)
[43] 1988 *CRC Handbook of Chemistry and Physics* 1998 69th edn pp E212–28
[44] Philips 2000 *WinGixa Software and User Manual* Philips Analytical X-Ray, Almelo, The Netherlands
[45] http://www.webelements.com
[46] Barna P B and Adamik M 1998 *Thin Solid films* **317** 27
[47] Patsalas P, Gravalidis C and Logothetidis S 2004 *J. Appl. Phys.* **96** 6234
[48] Ensiger W 1997 *Nucl. Instrum. Methods Phys. Res.* B **127/128** 796